Grain Moisture Sensing Using Electrical Capacitance Tomography

Ling Yu, Maomao Zhang, Dong Yang, Luke Loescher, and Manuchehr Soleimani

***Abstract*—Electrical Capacitance Tomography (ECT) is a non-destructive electrical imaging method used to visualise dielectric permittivity changes across a cross-section of a sample. This paper explores the effectiveness of ECT for moisture sensing in cereal grains, which plays a crucial role in determining grain quality and the likelihood of spoilage during storage. To achieve accurate and comprehensive insights into moisture distribution, tomography emerges as a promising technique due to its capacity to map larger areas and differentiate moisture variations with precision. Considering related research on the dielectric properties of grain, this paper systemically investigates factors known to affect permittivity. It evaluates ECT's ability to image moisture content relative to these influences. Experiments investigated how a sample's moisture, position, size, temperature, and density affect a sensor's ability to detect moisture changes. To date, limited research has focussed on these influences in the context of cereal grain moisture sensing with ECT. All the tests showed the reconstructions to produce results consistent with existing research concerning the dielectric properties of grain. This study concluded that ECT, utilised with a circular array, effectively distinguished between moisture content in reconstructed images, factors significantly affecting the results. ECT images were disturbed by the position and size of samples within the sampling area. The reconstructed images were also heavily dependent on the sample's bulk density and influenced by different moisture contents within the same sampling area.**

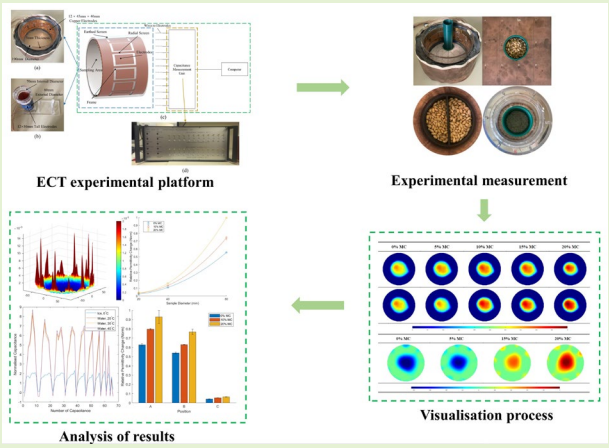

***Index Terms*—Electrical Capacitance Tomography, electrical imaging, moisture content.**

I. Introduction

MOISTURE content is a critical factor that affects the quality of cereal grains, such as wheat and barley [1]. Reduced moisture content improves food stability and minimises physical and chemical changes during storage [2]. According to the former study, it demonstrated that too high moisture content can result in germination and mildew for grain [3], while on the contrary, when the moisture content is too low, the physical structure of the grain will be compromised, and a reduction in the nutritional value of the grain [4]. Therefore, farmers must determine the moisture content of grain accurately and efficiently before and during storage and throughout the drying process to minimise losses.

Ling Yu and Maomao Zhang are with the School of Tsinghua Shenzhen International Graduate School, Shenzhen, China (e-mail: yul22@mails.tsinghua.edu.cn; zhangmaomao@sz.tsinghua.edu.cn).

Dong Yang is with Academy of National Food and Strategic Reserves Administration, Beijing, China (e-mail: yd@ags.ac.cn).

Luke Loescher, and Manuchehr Soleimani are with the School of Engineering Tomography Laboratory (ETL), Department of Electronic and Electrical Engineering, University of Bath, Bath, UK (e-mail: Luke.loescher@outlook.com; ms350@bath.ac.uk).

Various methods are available for measuring the moisture content of grain, which can be categorised as direct or indirect. The direct method involves weighing a known grain mass and drying it until its mass no longer decreases. The indirect method uses the electrical properties of grain to determine its moisture content, with resistance-based devices measuring the ability of compressed grain to conduct current, which increases as moisture content rises. Indirect methods may use either a meter or probe to take measurements, with probes being the only non-destructive option. Electrical Capacitance Tomography (ECT) is a non-destructive electrical imaging technique that can visualise the permittivity distribution of a cross-section of an object. In conventual ECT sensors, electrodes of typically eight to twelve in number are distributed outside an insulating frame that surrounds the desired sampling area, allowing for non-invasive imaging. Capacitance data is obtained between pairs of electrodes and processed to form an image. Non-conventional sensor arrays include square, conical, planar, and Electrical Capacitance Volume Tomography (ECVT) setups. ECT offers several advantages, including being non-invasive, low cost, simply implemented, and high-speed in image reconstruction [5]. ECT is a well-established tomography modality, continuously developed since the later 1980s, that finds applications in fluidised beds, pneumatic conveying systems, and combustion [6], [7]. Its low spatial

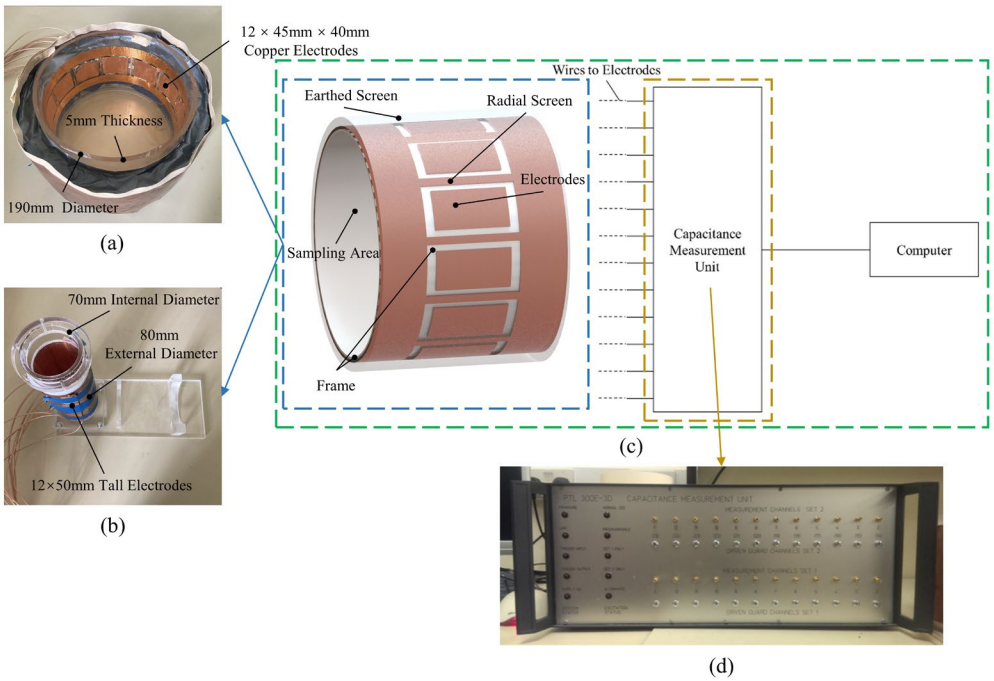

Fig. 1. Illustration of ECT system. (a) Photographs of Array A. (b) Photographs of Array B. (c) ECT main structure. (d)Photograph of PTL 300E-3D CMU.

resolution limits the technology, which depends on sensor design and image reconstruction [6]. ECT could be advantageous in mapping moisture variations across a wider sample, whether stationary or during conveyance.

ECT has been utilised across various applications for detecting dielectric changes in materials. These include studies using ECT for moisture detection. One such application, investigated by Voss et al., involved imaging moisture content in wood. They concluded that this modality is feasible for imaging water absorption and witnessed a constant increase in electrical permittivity where water had been infiltrated [1]. A similar positive correlation was found in soil moisture detection [8]. However, because of the mediums tested, neither of these studies was influenced by the significant impact of granular irregularities within the sample. Nevertheless, they provide a solid basis for showing ECT effectiveness in detecting moisture differences. Whilst studies on grains exist, these commonly focus on powdered or uniform samples which do not suffer from shape, size, or density variances. Research involving fluidised bed dryers with powdered grain or similar substances such as silica gel shows that ECT is sensitive to moisture and provides detailed information in the drying process [10], [11]. Limited research exists in the capacitance modality on whole grain moisture directly; however, studies have used cereal grains as samples for investigating granular flow. A paper from 2016 concluded that ECT could sense the concentration distribution of rice, the velocity distribution of air, and the change rate of permittivity from granular flow measurements in silos [11].

Grain moisture detection has been investigated more widely with alternative sensing technologies; these include microwave and radiofrequency sensing methods, which like ECT, are both rapid and non-destructive. One study found microwave sensors to determine soybean and wheat moisture with standard errors of 0.564% and 0.983%, respectively [4]. Similarly, radiofrequency was found to be a high-precision alternative and research shows it can produce moisture testing results within ±0.3% [12]. Whilst such research has shown both microwave and radiofrequency sensing methods to be effective for grain moisture detection, these technologies are generally more expensive and challenging to implement than ECT.

Whilst research exists surrounding ECT wet granule imaging, such as in fluidised bed drying, there is little work investing the applicability for grain moisture detection directly. This paper will, therefore, specifically focus on evaluating the effectiveness of ECT in measuring and imaging moisture content in cereal grains so that conclusions about its feasibility for industry application can be reached.

II. Experimental Rig of Grain with ECT

A. ECT System

Two sensor arrays were used during this research, shown in Fig. 1(a) and (b). Array A has twelve 45mm by 40mm copper electrodes distributed around the sensor frame. The sampling area is 190mm in diameter with a frame thickness of 5mm. Array B is 70mm in internal diameter and 80mm in external diameter. It has twelve 50mm tall electrodes around its periphery. Both sensor frames are made from acrylic. All the arrays have grounded conductors between the electrodes and radial shields. Array A and Array B are both circular arrays, the main difference being that Array A has a larger diameter. In this paper, Array A was used for experiments investigating the influence of sample position when a larger array diameter was required, while Array B was used for all other experiments.

Typically, ECT hardware includes three parts, a sensor array, a capacitance measurement unit (CMU) and a computer for data processing, illustrated in Fig. 1(c).

The CMU acquires mutual capacitance measurements. Only one electrode is excited during these measurements, and each subsequent electrode is used for detection individually. Therefore, for a typical twelve-electrode system, there are 66 individual measurements as demonstrated through the following equation, where N is the number of electrodes and M is the number of individual measurements:

$$M = \frac{N(N-1)}{2} \quad (1)$$

Capacitance was measured with the PTL 300E-3D CMU, shown in Fig. 1(d). This operates at a fixed frequency of 1.25MHz, which is the default operating frequency of the PTL 300E-3D CMU.

The Total Variation (TV) algorithm, used in this paper for image reconstruction, aims to minimize the total variation of the image by solving an optimization problem that balances fidelity to observed data and image smoothness [13]. The function outputs an image of size N, which was further processed in MATLAB to result in a colourmap where the gradient represents relative permittivity change.

B. Grain Samples

This paper used two grains, barley and rice, as samples for research. The initial moisture content of the two grains was obtained using the direct method. 50g of each grain was dried at 120°C in an oven and the weight was observed at 10-minute intervals until it stopped decreasing. The moisture contents were calculated using the following formula, where M_W is the wet mass and M_d is the dry mass:

$$M = \frac{M_W - M_d}{M_w} \times 100\% \quad (2)$$

Table I shows the results of this method. The moisture content of the barley and rice grains was calculated to be 12% and 10%, respectively.

Each grain was then portioned into five 250g samples. These were conditioned to 0%, 5%, 10%, 15%, and 20% moisture content. The samples were dried down to a specific mass for the 0%, 5%, and 10% moisture content samples; the rice sample at 10% moisture content did not require any conditioning. A mass of water was added to the 15% and 20% moisture content samples. The previously described moisture equation (2) was utilised to calculate the mass difference required for each moisture content. Each sample was manually mixed before being placed in a sealed bag and refrigerated for 48h to allow the water and grain to bond. The samples were returned to room temperature before measurement.

TABLE I
INITIAL MOISTURE CONTENT OF GRAINS

Grain	M_w (g)	M_d (g)	M (%)
Barley	50	44	12
Rice	50	45	10

C. Capacitance Measurements

The difference between the sample measurements and a reference set was found to produce images reflecting permittivity change. This was inputted into the TV function as f. To produce accurate and high-quality images, it was crucial to ensure that the position of these containers was constant across the measurements. The positioning map, illustrated in Fig. 2, was used for this purpose.

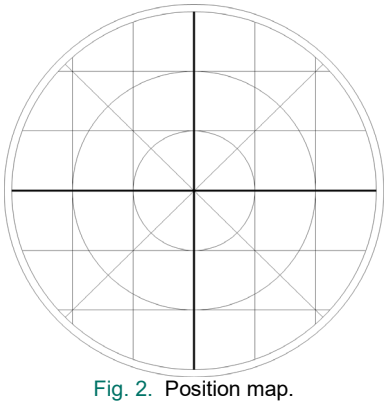

Fig. 2. Position map.

When capacitance measurements were taken, the CMU collected twelve data sets for the same samples. These measurements were then averaged to lessen the impact of background noise. As a hypersensitive imaging modality, any

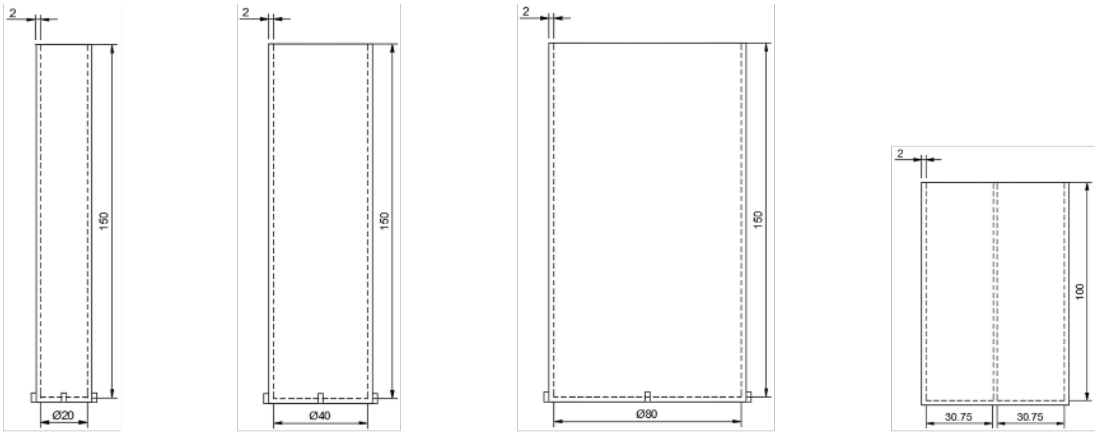

Fig. 3. Drawings of containers (mm)

external variations could significantly influence the precision of the results. Therefore, during all the experiments, persons stood away from the sensor and only a single sensor was operated at any time. Neither the temperature nor humidity of the lab changed significantly across the period of data collected.

III. Experimental Methods

This paper aims to evaluate the effectiveness of ECT in detecting moisture in cereal grains. The experiments focus on various factors that could affect the accuracy of ECT, including different types of cereal grains, positions within the sampling area, and the size of moisture pockets within the grain bulk. The study also investigates the relationship between moisture content and perceived permittivity, as well as the influence of temperature and bulk density on ECT's effectiveness. Overall, the goal is to determine whether ECT can effectively map permittivity across a range of moistures and provide accurate measurements for grain quality control.

A. Sample Containers and experimental setups

Each experiment utilised several 3D-printed cylinder containers, which were placed in the ECT. These are shown in Fig 3. Containers A, B and C were 20mm, 40mm and 80mm in inside diameter, respectively. All three were 1500mm in height and had a wall thickness of 2mm. They also held notches at the base to allow precise positioning relative to the sampling area. Container D was 100mm tall and segmented into two semi-circular volumes. All the capsules were printed out of PLA material.

During the experimental measurements, the sample grains were placed in containers, which had different dimensions. And then, the containers with the grains were placed in the ECT. As shown in Fig. 4.

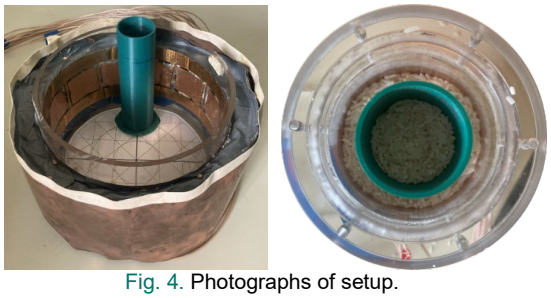

Fig. 4. Photographs of setup.

B. Sample moisture type, position, and size

This experiment was repeated with a circular array, Array B. The container was placed in the centre of each array, in an air background, and the empty container was used for reference measurements. And then, repeat the experiment by changing the type, position, and size of the sample separately.

C. Sample variation

This methodology aimed to assess the ability of ECT to detect changes in permittivity where the sample is split with moisture content. Which fits inside Array B, the sampling area was divided into two equal parts. One side of the container was filled with barley at 0% moisture, while the other side contained barley that varied between 0% and 20% moisture content. The grain was loosely filled and a reference measurement was taken when the container was empty. The methodology was then repeated with a 20% moisture content sample as the constant.

Another methodology investigated the impact of concentric moisture variations. The container was positioned in the centre of Array B and filled with rice, varying from 0% to 20% moisture content. The background for this experiment was rice at a 10% moisture content of 15mm in a depth encircling Container. All the grain was loosely packed. The image reconstruction was taken with reference data when the container was filled with rice of 10% moisture.

D. Sample density

The density of each moisture sample, ranging from 0% to 20%, was consistently maintained at 0.769 g/cm³ within the specified container volume. The original bulk densities for various moisture levels, referred to as "loose density," are detailed in Table II . The densities of samples at 0%, 5%, and 10% moisture content are identical, whereas samples with 15% and 20% moisture content exhibit lower densities. Consequently, to uphold uniform densities for testing samples with varying moisture levels, it is necessary to compress the 15% and 20% moisture content samples into the container.

Another methodology evaluates the relationship between relative permittivity change and variance in bulk density in ECT imaging. Array B was used and split into two equal segments with Container. Initially, barley at 10% moisture was placed into the container. Both sides of the container were filled to the top with the same grain mass. Whilst the right-hand side remained constant in bulk density, the opposite side was compressed in 25mm intervals to produce a range of bulk density samples. This was then repeated for barley at 20% moisture. Reference measurements were taken when the container was empty.

E. Sample temperature

This experiment used Array B. The container was positioned in the centre of the array and filled with tap water, which was prepared to temperatures of 20°C, 30°C, and 40°C. These temperatures were confirmed with a Duratool digital thermometer. An additional sample was taken where the water was frozen. The empty container was used as a reference, and only a single data set was used for this experiment.

TABLE II
ORIGINAL BULK DENSITIES (G/CM³) OF DIFFERENT MOISTURE

Sample	0% MC	5% MC	10% MC	15% MC	20%MC
Barley	0.769	0.769	0.769	0.748	0.695
Rice	0.806	0.806	0.806	0.759	0.743

TABLE III
IMAGE RECONSTRUCTION RESULTS OF DIFFERENT MOISTURE

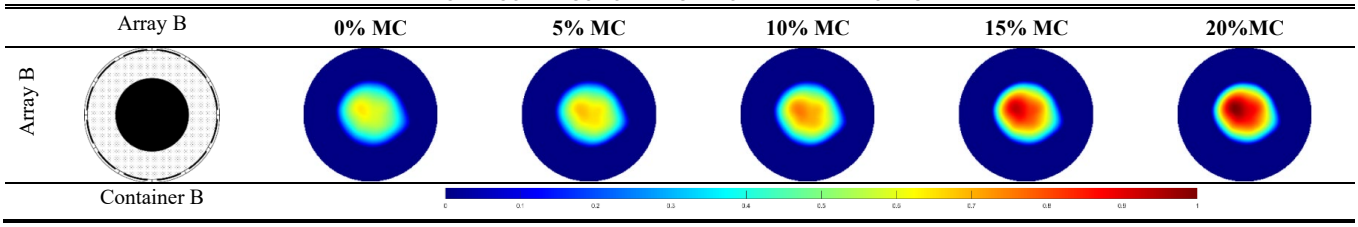

IV. EXPERIMENTAL RESULTS AND DISCUSSION

A. Sample moisture

The reconstructed images were averaged across each test repetition. Table III presents the resulting images, where the reconstructions are shown relatively per array. As such, red colours show areas of elevated relative permittivity change relative to the other images, and blue colours convey minimal relative permittivity change. A scale is tabled, per relative reconstructions, to enable quantification. As stated previously, the reconstructed images depend on the TV inputs; here, parameters were chosen to produce the highest-quality reconstructions across the range of images. The illustrations in the first column represent scale; the black area shows the experiment's sample.

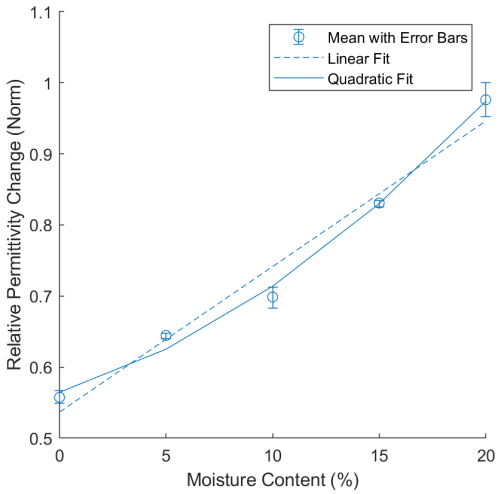

Fig. 5. Relationship between relative permittivity change (Norm) and moisture content.

In Figure 5, the plot shows a significant increase in relative permittivity change as the moisture content increases. The relative permittivity of water typically exhibits a significantly greater magnitude than that of most grains. Consequently, as the moisture content within the grains, the difference between the relative permittivity of the grains and the surrounding air becomes more pronounced. This yields a more substantial in the relative permittivity change as measured through the technique of ECT. Data points were fitted with both linear and quadratic curves. The linear fit yielded R2 (R-Square) and RMSE (Root Mean Squard Error) values of 0.9690 and 0.0259. While the quadratic fit resulted in R2 and RMSE values of 0.9940 and 0.0114, which are in proximity to 1 and 0, respectively. This suggests that the quadratic curve model provides a superior explanation for the observed data variations and outperforms the linear curve. And quadratic curve fitting is used in all of the latter.

The values in Fig. 5 are expressed in terms of the 2-norm value and are calculated by the following equation:

$$norm(x) = \sqrt{\sum_{i=1}^{n} \left(\frac{x_i}{\max(x)}\right)^2} \tag{3}$$

where $norm(x)$ is the normalized 2-norm value, and x_i is the relative permittivity value.

The circular array exhibited great sensitivity to changes in moisture content and produced distinguishable measurements and images between the five moisture samples. The sensor showed relatively small variations in the results, allowing for precise imaging. These conclusions demonstrate that ECT, applied with circular arrays, is effective for grain moisture sensing. The results show that any potential differences in water composition, bound or free, do not significantly limit the effectiveness of ECT. The obtained results also agree with conclusions from reviewed studies linking permittivity and moisture content.

B. Sample type

The results are shown in Table IV , alongside the initial barley images. There is no difference in image quality between the two samples; both are well-defined in shape and size. However, a small visual contrast is seen between barley and rice grains across the moisture range, where rice displays a more significant relative permittivity change.

This confirms that grain permittivity differs per grain type and subsequently affects ECT measurements. This is consistent with existing research and is linked to grain density which is considered elsewhere in this paper. The results also suggest that the correlation between permittivity and moisture content changes with grain type. Consequently, any application would need to consider grain-type calibration.

TABLE IV
IMAGE RECONSTRUCTION RESULTS OF DIFFERENT CEREAL GRAINS

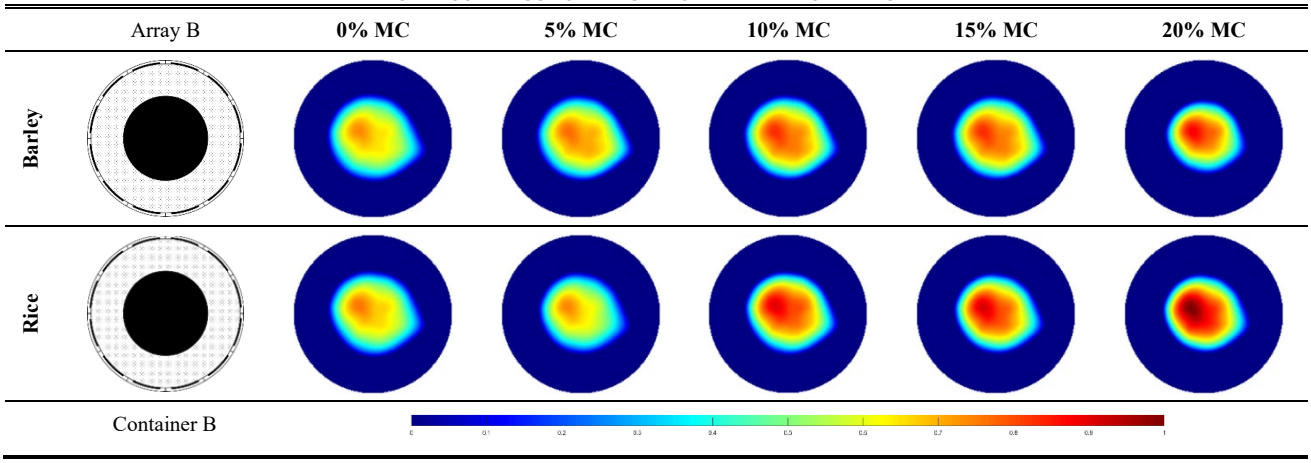

TABLE V
IMAGE RECONSTRUCTION RESULTS OF DIFFERENT POSITIONS WITHIN THE SAMPLING AREA

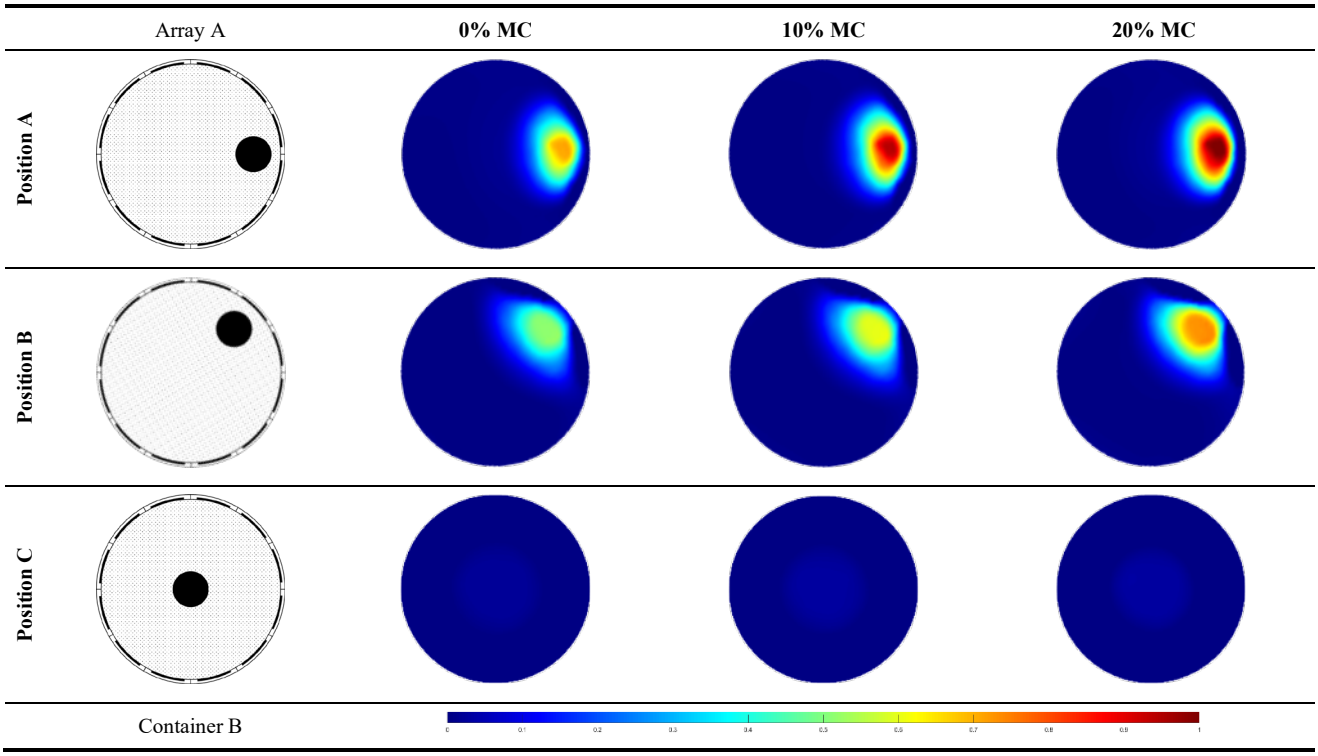

C. Sample position

The reconstruction process produced a total of nine images. These are tabled in Table V, which shows that the position of the sample significantly impacted the relative change in permittivity. As a result of being relative to each other, the images obtained in Position C have low contrast as the permittivity change is relatively small compared to those observed in Position A and Position B. Accurately positioned and relatively well-defined images were produced for all three positions. The shape of sample reconstructions was less representative at the edge of the sampling area.

Extracting the numerical data from these images allows for further comparative analysis. Fig. 6 shows the 2-norm values of each reconstruction, including the variation from the three experimental repeats. The impact of position changes on permittivity is more significant than the moisture content of the barley. For example, the highest moisture sample in the centre of the sampling area is only 4.5% of the permittivity change recorded at the periphery, directly in front of an electrode. Critically, the change in permittivity due to moisture is significantly weakened in Position C, where the relationship is negligible relative to Position A or Position B.

In ECT, the sensitivity map is a parameter used to describe the distribution of sensitivity of capacitance to permittivity imaging. The expression for the sensitivity is as follows:

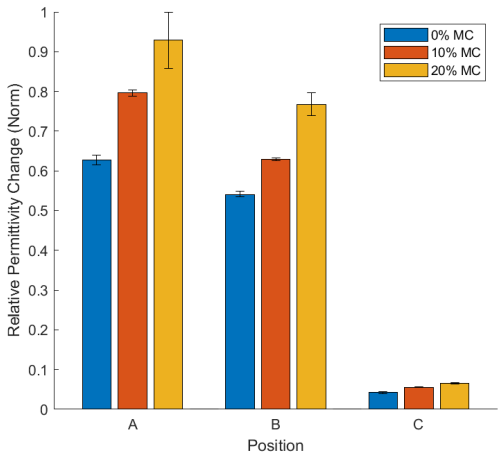

Fig. 6. Charted image reconstruction result of different positions within the sampling area.

$$S_{ij} = \frac{\Delta C_{ij}}{\Delta \varepsilon} \approx -\frac{\int_{\sigma} \nabla \varphi_i \cdot \nabla \varphi_j ds}{V^2} \quad (4)$$

where S is the sensitivity, C is the Capacitance, ε is the relative permittivity change, and φ is the value of the voltage applied to the i, j pole plate as V.

In Fig. 7(a), the results of the summation of the 66 sensitivity maps are schematically illustrated. The sensitivity near the electrodes is higher than the centre region. The average sensitivity of the three regions of positions A, B, and C are plotted in Fig. 7(b). Position A corresponds to the dark red peak, position B is the valley between the two peaks, and position C is the dark blue trough in the centre. The sensitivity at position A is slightly higher than position B, but much bigger than position C, which also matches the permittivity results in Fig.4. Therefore, for better imaging quality of the moisture distribution, the ECT sensor should not be too large compared with the sample size, i.e., the sample won't be relatively far from the electrodes to decrease the sensitivity.

D. Sample size

Table VI shows the image reconstructions for each container at each moisture content. It is evident that size is critical in the ability of ECT to detect changes in permittivity. While the relativeness of the images makes it difficult to observe the actual permittivity change in the smaller samples, all the images are clear and distinct in shape and position. The reconstructions for both Container C and Container B are representative in size. However, in the reconstructed images for Container A, these samples appear larger than they are.

The 2-norm values of the reconstructions, shown in Fig 8, support the visual trends. The figure highlights that sample diameter has an increasingly positive correlation with relative

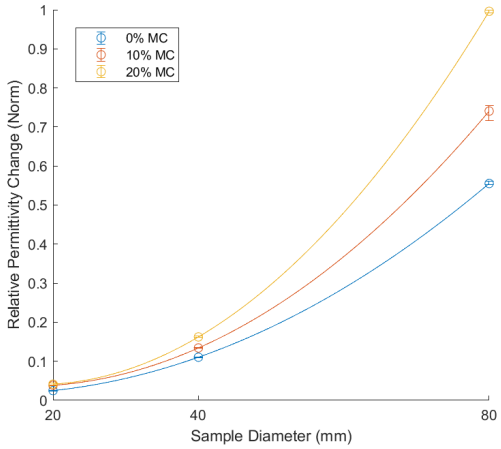

Fig. 8. Relationship between relative permittivity change (Norm) and different size within a grain bulk (norm).

permittivity change. The effect of moisture becomes less prominent in smaller samples. One important finding is that the permittivity change for the 10% moisture content sample is higher than that of the 20% sample at a diameter of 20mm.

The presented results indicate that ECT is ineffective in detecting permittivity changes in small samples and is increasingly less sensitive to moisture changes as size decreases. This is because smaller samples will interact with fewer electric field lines and produce less information through capacitance measurements. Therefore, any application would be limited by a minimum detectable area.

E. Sample variation

1) *Different split moisture variations*

The images in Table VII show the reconstructions across the measured moisture range. The images accurately reflect moisture content increasing in half of the sample where this is variable. As expected, the fifth and sixth images are nearly identical since they are effectively the same sample. The first

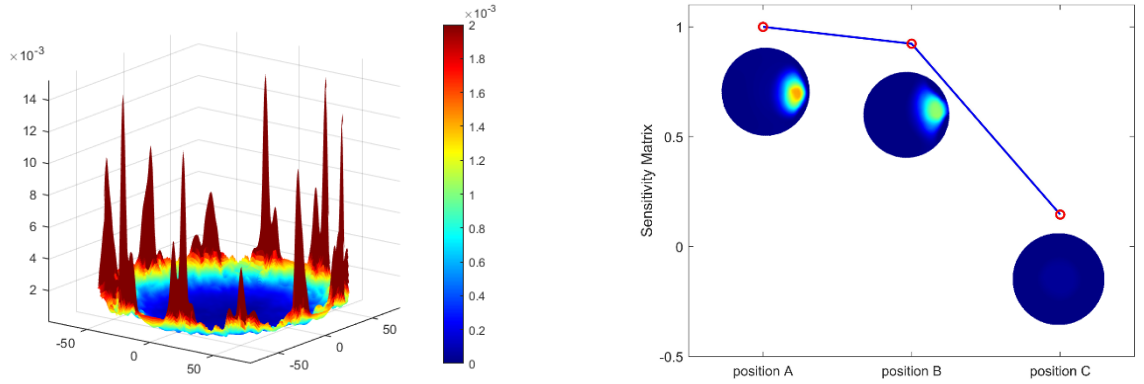

(a) (b)

Fig. 7. Sensitivity analysis:(a) Summation of 66 sensitivity maps; (b) Sensitivity at the sample location.

TABLE VI
IMAGE RECONSTRUCTION RESULTS OF DIFFERENT SIZE WITHIN A GRAIN BULK

Array A	0% MC	10% MC	20% MC
Container A	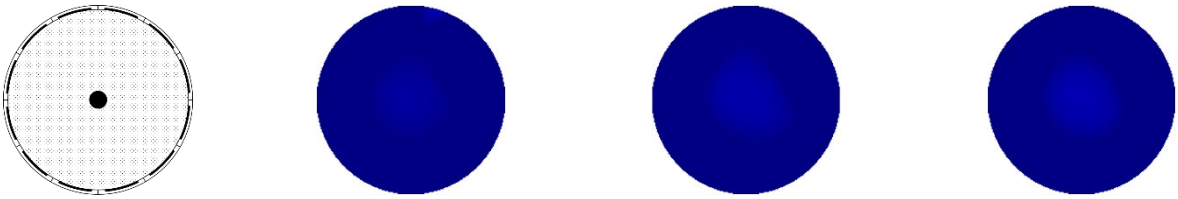		
Container B	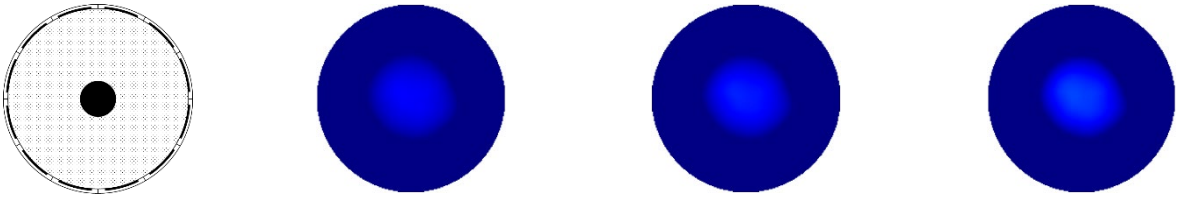		
Container C	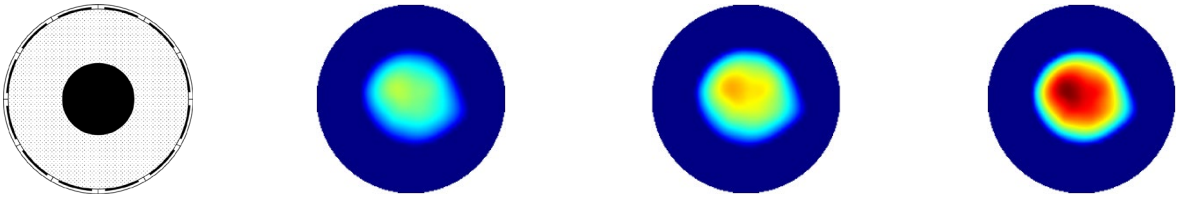		

TABLE VII
IMAGE RECONSTRUCTION RESULTS OF DIFFERENT SPLIT MOISTURE VARIATIONS

Array B	0% MC	5% MC	10% MC	15% MC	20% MC
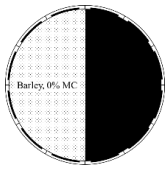					
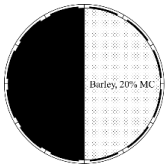					
Container D					

TABLE VIII
IMAGE RECONSTRUCTION RESULTS OF DIFFERENT CONCENTRIC MOISTURE VARIATIONS

Array B	0% MC	5% MC	15% MC	20% MC
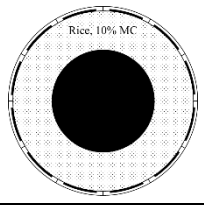				
Container B				

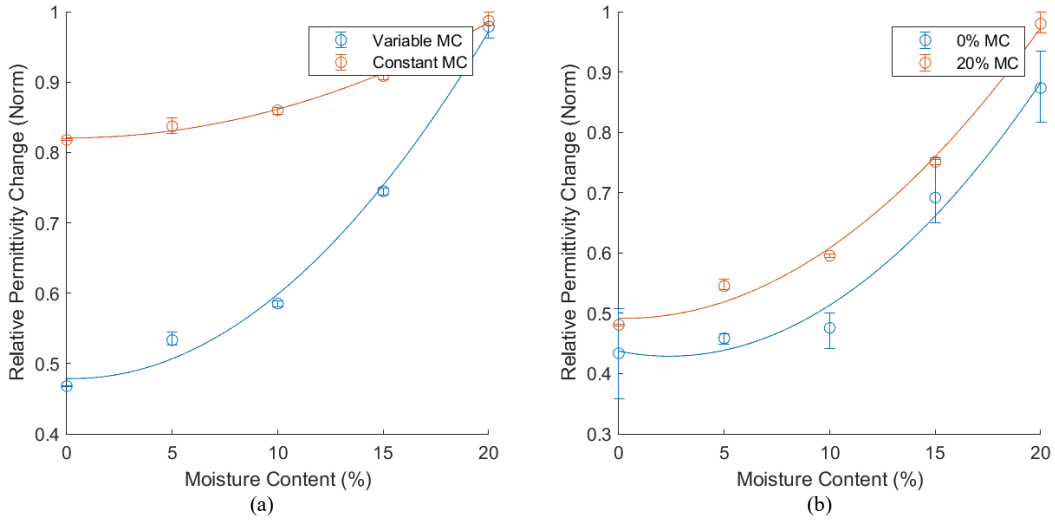

Fig. 9. Relative permittivity change (Norm) of different split moisture variation: (a)The constant and variable halves of the images; (b) The variable halves for both 0% and 20% moisture content.

and final images, where the grain moisture is constant across the sample, show a more noticeable permittivity change on the left-hand side. This difference could be due to a sensor-related issue, as the error appears constant across the measurements. Left in Fig. 9 plots the 2-norm values for the constant and variable halves of the images, where the constant barley was at a 20% moisture content. The x-axis represents the moisture content of the variable half. The permittivity trend for half of the sample that increases in moisture content closely resembles the relationship found in the first experiment. The graph also shows that the permittivity of the constant half appears to have a weak quadratic dependence on the moisture content of the variable half; in reality, the permittivity remains constant. On the right-hand side of Fig. 9 . The two curves appear parallel, demonstrating that the 0% and 20% constant halves have the same effect upon higher and lower moistures, respectively.

Crucially, for the 0%, 5%, and 10% moisture samples, the permittivity change measured cannot differentiate between moisture variations due to the difference in the y-intercept of the two curves.

2) *Different concentric moisture variations*

Table VIII. Image reconstruction results of different concentric moisture variations. shows the relative reconstructions obtained. Since the reference measurement was at 10% moisture, the reconstructed images include positive and negative relative permittivity changes. The influence of concentric grain moisture distorts the image shape, as seen most notably in the 20% moisture sample. Despite this, all the images effectively differentiate the inner changes in permittivity arising from moisture differences and all are generally well-defined.

Fig. 10 graphs the average of the data in the centre of the images. Due to the reference measurement was at 10% moisture, only four points are shown in the graph. This demonstrates a strong relationship between inner moisture and permittivity change, like the relationships seen in previous experiments.

TABLE IX
IMAGE RECONSTRUCTION RESULTS OF DIFFERENT BULK DENSITY (SPLIT CHANGES)

Array B	0mm	5mm	10mm	15mm	20mm
	Bulk Density Increase →				
	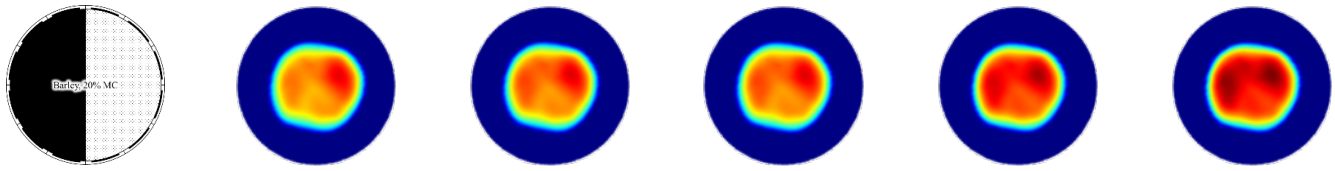				
Container D	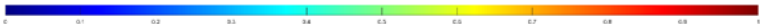				

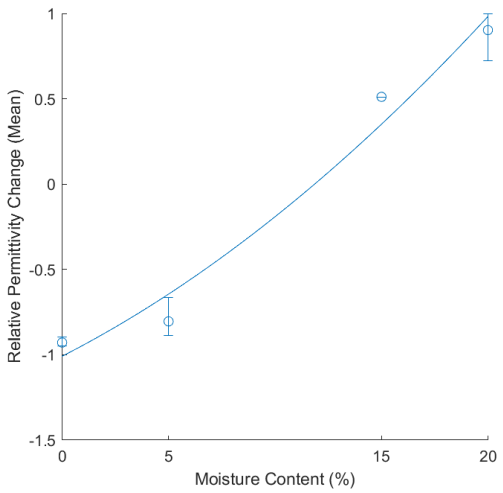

Fig. 10. Relationship between relative permittivity change (Norm) and different concentric moisture variations.

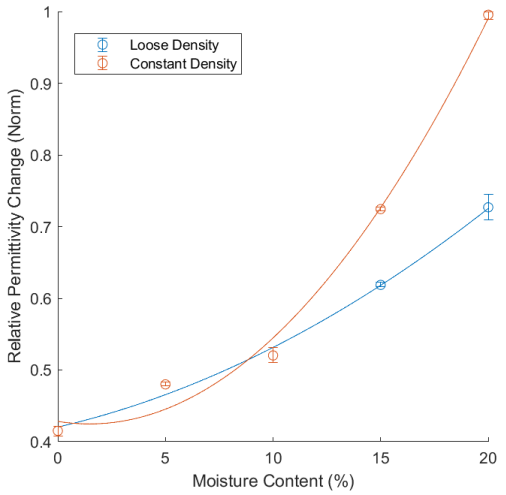

Fig. 11. Relationship between relative permittivity change (Norm) and different bulk density (uniform changes).

These results indicate that split moisture variations within the sampling area reduce ECT's ability to detect moisture differences. Due to the quadratic relationship between moisture content and permittivity, ECT is more limited at lower moistures, where moisture variations can make distinguishing between moistures challenging.

The concentric experiment results demonstrated that ECT is not limited in this regard, no matter if the periphery of the sample area is high or low in moisture relative to the centre of the sample.

F. Sample density

1) *Effect of uniform changes in bulk density on ECT*

Fig. 11 presents the impact of moisture content on perceived relative permittivity for both loose density and constant density barley samples. The 2-norm image values show that the constant density caused an increase in measured permittivity at 15% and 20% moisture, where the samples were comparatively denser. The relative difference of this increase appears to rise with higher moisture content. Critically, the constant density measurements, where grains of varying moisture contents are compressed to the same density, taken at 15% moisture show a similar permittivity change to those observed at 20% moisture content in their natural state without compression, known as loose density.

2) *Effect of split changes in bulk density on ECT*

Table IX shows the image results from this methodology. These reconstructions show the variable bulk density on the left and the constant bulk density on the right-hand side. As anticipated from previous experiments, the sample with 20% moisture content shows a visually more significant change in relative permittivity. While differences in bulk density are not visually prominent, variances in permittivity are seen in the profiles. Consistent with previous sensor measurements, the array shows a greater permittivity change on one side, regardless of a change in bulk density; this somewhat distorts the image results.

Fig. 12 shows the 2-norm permittivity values of the left-hand side of the image. The correlation between bulk density and permittivity is much more apparent and shows a positive quadratic relationship. The plot shows an increased relationship when the moisture of the grain is higher.

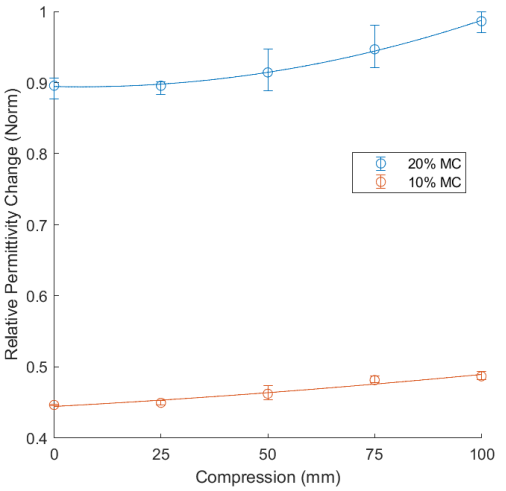

Fig. 12. Relationship between relative permittivity change (Norm) and raw data results of different bulk density (split changes).

These results show that bulk density significantly impacts the measured capacitance and therefore imaged permittivity. Both experiments show higher relative permittivity changes for samples with greater bulk density or compression. When bulk density increases, the space between grains reduces. Therefore, the shown relationship is expected because the grains, particularly at higher moisture contents, have a higher permittivity than air. The results in Figure 9 suggest that density differences can be equally or more significant than moisture differences, limiting ECT's effectiveness for moisture imaging. This is significantly limiting at higher moisture contents, as the relative permittivity and the rate of change in permittivity due to bulk density changes are notably affected by moisture content.

G. Sample temperature

Fig. 13 shows the results of this methodology. Despite being at different temperatures, there is a minimal difference between

the water measurements. The ice capacitance measurements are distinguishable from the water samples and have significantly lower normalised capacitance values at separated electrodes.

Whilst ice is mainly irrelevant to grain moisture applications, the results show that ECT effectively detects ice against water. The CMU used operates at a frequency of 1.25MHz, and in agreement with existing research, appears incapable of distinguishing permittivity changes in water because of temperature. This is advantageous for sensing differences in grain moisture as the capacitance measurements would not be influenced by the range of temperatures often observed. However, this conclusion is limited to the temperature range experimented with in the paper.

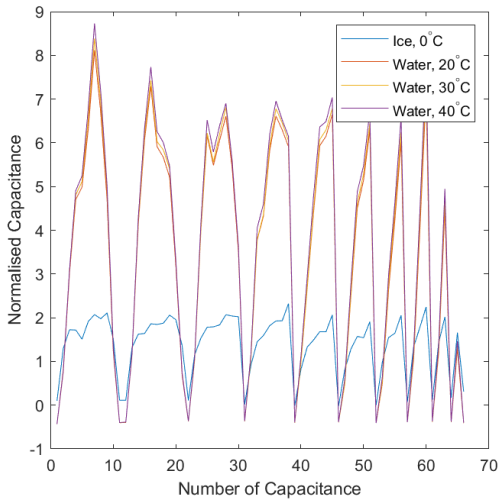

Fig. 13. Raw data results of different concentric moisture variations.

V. Conclusions

Considering related research on the dielectric properties of grain, this paper systemically investigates factors known to affect permittivity. It evaluates ECT's ability to image moisture content relative to these influences. Experiments investigated how a sample's moisture, position, size, temperature, and density affect a sensor's ability to detect moisture changes. The main conclusions are as follows:

(1) The results indicate that ECT has a good performance in measuring the water content of grains, as potential differences in water composition, whether bound or free, do not significantly limit its effectiveness.

(2) Grain permittivity varies depending on the type of grain, allowing for differentiation between different grains using ECT measurements.

(3) The position of samples within the sampling area has a significant impact on ECT measurements. The sensitivity of ECT measurements varies in different regions, and a well-designed sensor can be optimized for specific applications.

(4) ECT may have limitations in detecting permittivity changes in small samples and becomes less sensitive to moisture changes as the size decreases. This is because smaller samples interact with fewer electric field lines and provide less information through capacitance measurements. To optimize the performance of ECT sensors, it is advisable to minimize the differences in diameter between the ECT sensor and the object being measured, thus ensuring more accurate and reliable results.

(5) ECT is able to image the moisture variation within the sensing area of different distributions including the split or the concentric in our case.

(6) Measured capacitance is significantly influenced by bulk density, with higher relative permittivity changes observed in samples with greater bulk density or compression.

(7) ECT is effective in detecting the presence of ice as opposed to water.

This paper demonstrates the feasibility of using ECT for grain moisture detection in static imaging mode. ECT is well-known for its advantage in imaging materials in transition, providing hundreds of frames per second. Thus, it could be a great device for grain inspection on conveyor belts or at the exit port of grain tank silos. Machine learning applications can be developed for such applications in future studies. For instance, machine learning models are applied to analyze real-time data collected by ECT sensors for tasks such as anomaly detection and classification. Additionally, these models can optimize the parameters of ECT sensors to enhance accuracy and overall performance.

In brief, this paper systematically investigates factors affecting permittivity in grain, demonstrating that ECT effectively measures grain moisture content, differentiates grain types, and is sensitive to sample position, size, temperature, and density. It also highlights ECT's potential for grain inspection in static imaging mode, suggesting machine learning applications for real-time data analysis and sensor optimization.

References

[1] C. V. Ratnavathi and V. V. Komala, “Sorghum Grain Quality,” in Sorghum Biochemistry, Elsevier, 2016, pp. 1–61.

[2] X. Liu, X. Chen, W. Wu, and G. Peng, “A neural network for predicting moisture content of grain drying process using genetic algorithm,” Food Control, vol. 18, no. 8, pp. 928–933, Aug. 2007.

[3] V. Giannetti, M. Boccacci Mariani, and S. Colicchia, “Furosine as marker of quality in dried durum wheat pasta: Impact of heat treatment on food quality and security – A review,” Food Control, vol. 125, p. 108036, Jul. 2021.

[4] C. Li, C. Zhao, Y. Ren, X. He, X. Yu, and Q. Song, “Microwave traveling-standing wave method for density-independent detection of grain moisture content,” Measurement, vol. 198, p. 111373, Jul. 2022.

[5] C. Yossontikul, K. Chitsakul, M. Sangworasil, and Y. Kitjaidure, “An electrical capacitance tomography,” in 6th International Conference on Signal Processing, 2002., Aug. 2002, pp. 1766–1769 vol.2.

[6] F. Wang, Q. Marashdeh, L.-S. Fan, and W. Warsito, “Electrical Capacitance Volume Tomography: Design and Applications,” Sensors, vol. 10, no. 3, pp. 1890–1917, Mar. 2010.

[7] W. Yang, “Design of electrical capacitance tomography sensors,” Meas. Sci. Technol., vol. 21, no. 4, p. 042001, Apr. 2010.

[8] A. Voss, A. Seppänen, S. Siltanen, L. Salokangas and D. Baroudi, “Imaging of moisture content in wood using electrical capacitance tomography,” in World Conference on Timber Engineering, Vienna, 2016.

[9] N. B. Abd. Karim and I. Bin Ismail, “Soil moisture detection using Electrical Capacitance Tomography (ECT) sensor,” in 2011 IEEE International Conference on Imaging Systems and Techniques, May 2011, pp. 83–88.

[10] A. Sdayria, F. Ouled Saad, J. Sghaier, A. Nissinen, M. Vauhkonen, and A. Elcafsi, “In-Line Monitoring of Drying Kinetics of a Fixed Bed Using an Electrical Imaging Technique,” Dry. Technol., Feb. 2015.
[11] J. L. Zhang, M. X. Mao, J. M. Ye, H. G. Wang, and W. Q. Yang, “Investigation of wetting and drying process in a gas-solid fluidized bed by electrical capacitance tomography and pressure measurement,” Powder Technol., vol. 301, pp. 1148–1158, Nov. 2016.
[12] J. Jia, Y. Yang and H. McCann, “Granular Flow Measurement in Silos Using Electrical Capacitance Tomography,” in 7th International Symposium on Process Tomography, Dresden, 2016.
[13] Z. Chen, W. Wu, J. Dou, Z. Liu, K. Chen, and Y. Xu, “Design and Analysis of a Radio-Frequency Moisture Sensor for Grain Based on the Difference Method,” Micromachines, vol. 12, no. 6, p. 708, Jun. 2021.
[14] J. F. P.-J. Abascal et al., “Fluorescence diffuse optical tomography using the split Bregman method: fDOT using the split Bregman method,” Med. Phys., vol. 38, no. 11, pp. 6275–6284, Oct. 2011.